OCTAHEDRON
Drug Research
Vol. 5
Research Article

A novel approach for apoptosis and caspase-3 inhibition using new candidates of 1,5-Diaryl triazole-3-carboxamides

Adel M. Abdelhakem, [1*] El-Shimaa M. N. Abdelhafez, [1] Samar H. Abbas, [1] Sara Mohamed Naguib Abdel Hafez, [2] Walaa Yehia Abdelzaher, [3] Omar M. Aly, [4]

[1] Department of Medicinal Chemistry, Faculty of Pharmacy, Minia University, Egypt,
[2] Department of Histology and Cell Biology, Faculty of Medicine, Minia University, Egypt,
[3] Department of Pharmacology, Faculty of Medicine, Minia University, Egypt
[4] Department of Medicinal Chemistry, Faculty of Pharmacy, Port Said University, Egypt
[*]Correspondence: pharmacist_adel2010@yahoo.com, Postal address: 61722

.ARTICLE INFO

Article history :
Received 5 May 2024
Received in revised form
31 May 2024
Accepted 31 May 2023
Available online 1 June 2024

Keywords: Antiapoptotic; 1,2,4-triazole-3-carboxamide; Caspase-3; NAC; Histopathology; Immunohistochemistry; Liver; Ovary; Docking.

ABSTRACT

Decreasing or inhibiting apoptosis is a therapeutic strategy to reduce the pathological states of diseases like stroke, neurodegeneration, retinal cell death, myocardial and liver ischemia, and inflammatory diseases such as sepsis, osteoarthritis, rheumatoid arthritis, and asthma. This study aims to design and synthesize a new series of apoptosis inhibitors using a 1,5-diaryl-1,2,4-triazole3-carboxamide scaffold. Then we conducted a comprehensive assessment of the effects of compounds **8a, 8b, 9a, 10a,** and **10b** on two critical organs: the liver and ovary.. *In vivo,* general biomarkers in the liver and ovary were measured and specific biomarkers were. Different stains such as Perl's iron stain, H & E stain and immune stain were utilized to evaluate caspase-3 inhibition. The findings are consistent with the docking study, i.e., compounds with two carbon linkers are better than those with longer or shorter ones as antiapoptotic. The most promising compounds **8a** and **10a** showed the highest potencies and selectivity against caspase-3 amongst other caspases like caspase -7, -8, -9, and 10 that could be considered for further clinical studies.

1. Introduction

Apoptosis is a form of cell death in which a programmed sequence of events leads to the elimination of cells [1]. Although apoptosis occurs typically during development and aging as a homeostatic mechanism to maintain cell populations in tissues, it is represented as a defense mechanism in immune reactions or when cells are damaged by diseases or noxious agents [2]. Too little or too much apoptosis due to imbalance probably occurs in some cases between apoptotic and antiapoptotic mediators leading to some diseases that are attributed to overexpression or inhibition of apoptotic mediators [2]. When apoptosis does not work correctly, cells that should be eliminated may persist and become immortal, for example, in cancer and autoimmunity [3, 4]. When apoptosis works overly well, it kills too many cells and inflicts grave tissue damage; this is the case in strokes[5] and neurodegenerative disorders such as Alzheimer's [6], retinal cell death [7], myocardial and liver ischemia [8, 9], inflammatory diseases such as sepsis [10], osteoarthritis [11], rheumatoid arthritis [12], and asthma [13]. The Caspase family is a hot target for drug design because dysregulation of caspase expression leads to severe diseases. To date, 14 mammalian caspases have been identified, among them, caspases -2, -3, -6, -7, -8, -9, and -10 which were described as apoptotic caspases [14]. The nucleophilic cysteine in the caspase active site is involved in breaking down aspartic acid peptide bonds within proteins [3]. Caspase-3 is generally more promiscuous than caspase-7 and is revealed as the major

executioner of space during the demolition phase of apoptosis [15, 16]. Additionally, caspase-3 plays a key executioner role,e and its inhibition can drastically prevent apoptosis *in vitro* and *in vivo* [14].

Liver ischemia is a life-threatening disease that may occur due to abnormal heart rhythms, heart failure, dehydration, sepsis, severe bleeding, blood clotting in the hepatic artery during liver transplantation, burns, and blood vessel swelling [17]. Ovary ischemia is one of the leading causes of polycystic ovary syndrome, the most common cause of ovulatory infertility in about 10% of women of childbearing age [18-20]. Ischemia/reperfusion (I/R) injury is the restoration of blood supply to organs after an ischemic period leading to parenchymal damage due to exaggerated apoptosis [21]. I/R injury elevates mortality rates to 60–80%. Because of the emergence of acute hepatic and ovarian ischemia and its ongoing impact on the global health system, there has been a growing interest in developing novel antiapoptotic agents to combat this disorder. As a result, we here reported our medicinal chemistry efforts, starting from the core scaffold of caspase inhibitors to the design of simpler and more efficient antiapoptotic compounds simulating the general structure of caspase inhibitors as illustrated in **Figure 1**. Most caspases recognize tetrapeptide sequences from the *N*-terminus to the *C*-terminus, positions of each residue on the existing substrate that could be named P4, P3, P2, and P1. The corresponding binding sites on the protein are named S4-S1[22, 23]. The enzyme can hydrolyze the peptide bond after the P1 Asp [24]. Throughout the designed structure, **P1** was designed to be a straight-chain aliphatic carboxylic acid with different lengths. This provides more flexibility for the COOH group, which acts as a cysteine trap, to be more available for interaction with the suitable amino acid residues in the binding site of caspase. While **P2** was designed to be 1,2,4-triazole; triazole incorporation in some compounds increases the caspase inhibition activity as in compound **I** with IC_{50} = 84.9 nM when H1,4-disubstituted-1,2,3-triazole replaces H atom gave compound **II**, the inhibitory activity improved to be with IC_{50} = 9 nM for caspase-3 inhibition and as in case of Ald-SC-2, compound **III**, with IC_{50}= 4.67 μM [25].

Another objective of this study was to identify the effect of **P3** and **P4** on inhibitory activity by trying *para*-substitution on ring **A** and the addition of ring **B** to increase the inhibitory activity of the designed compounds (**Figure** S**2)**.

2. Results and discussion

2.1. Docking study

The target compounds, 1,2,4-triazole-3-carboxamide derivatives of different substituents on ring A with different lengths (X=1-5) (**Figure 2**), NAC as a reference drug and the caspase 3 co-crystalized ligand NA3 ((3S)-3-{[(5-bromopyridin-3-yl)carbonyl]amino}-4-oxobutanoic acid) were docked on caspase-3 protein (PDB: 1re1) [26]. The more the binding, the more caspase inhibitory activity and the more antiapoptotic activity along with the affinity and the value of the root-mean-square deviation of atomic positions (rmsd), which indicates the better fit and more stability of the compound conformation into the pocket [27, 28]. Based on the validation process, the obtained (rmsd) is 1.3341 Å. It is less than 2 Å indicating that the docking protocol with the receptor (PDB code: 1RE1) is valid and feasible for the advanced docking process. Docking results revealed that compounds of the linker 2 carbons i.e., carboxamides of 3-amino propionic acid (β alanine), are the best in affinity to the binding site of caspase 3. In an attempt to explain the highest potency of **10a** which is lower in affinity than **8a, 9a and 10d. 10a** is a prodrug as it is an ester. Its carboxylate form was docked and the res, ults were impressive high-affinity E_conf -69.9612 kcal/mole while the ester form E_conf is 8.8229 kcal/mole. In addition to S-the final score, rmsd_refine between the pose before and after refinement, E_conf-The energy of the conformer, The interaction with the catalytic site of caspase 3, Cys 285 and His 237 was highly considered (**Figures 1** and S**3**). Compounds 8a, 9a, 10a(a) and 10a showed binding with the caspase-3 catalytic binding site (Cys 285 and Hist 237) and NAC and NA3. The docking results revealed that all compounds 8a,9a, 10a, NA3 and NAC showed similar bondings. O- of carboxylate formed ionic bonds with Arg(A) 179, and Arg(B) 341. C=O, the carboxylic group, showed interaction with Cys(A)285. The amidic carbonyl played as a hydrogen bond acceptor with His(A) 237. Triazole ring showed pi-cation interaction with His(A) 237. Compounds **8b**, 10b, 9b and **10b** did not show good binding with the catalytic site as they did not form binding with His(A)237.

2.2. Chemistry

Based on the docking study, compounds **8a, 9a, and 10a** may have expected good antiapoptotic effects, while **8b, 9b,** and **10b** with low or no activity. At the same time, compounds of linkers of the length (x= 1, 3, 4 or 5) may be of partial activity. So, compounds of the expected high activity like **8a**, **9a**, **10a** and the lowest activity **8b** and 10 **b** were selected to save time and money. The target 1,2,4-triazole-3-carboxamide derivatives **8a, 8b, 9a, 10a** and **10b**) and their intermediates were prepared as outlined in **Scheme 1**. According to Schotten-Baumann, a nucleophilic substitution reaction was carried out throughout the acylation of glycine with benzoyl chloride, producing one equivalent 2-(benzamido)acetic acid **5**. Erlenmeyer azlactone synthesis of oxazolone intermediate

6 was performed through intramolecular condensation in a dehydrating agent such as acetic anhydride.[29, 30]

Treatment of appropriate aniline derivatives with the nitrosonium ion generated *in situ* upon the reaction of sodium nitrite with HCl at 0 ºC afforded the corresponding diazonium salt **2a, 2b** and **2c** [31]. According to the Kuskov-like reaction, coupling of the diazonium salts **2a**, **2b,** and **2c** with the active methylene carbon of lactone **6** in the presence of sodium acetate afforded hydrazone derivatives **7a,7b** and **7c** in 75-85% yield. Based on Sawdey rearrangement, refluxing the mixture of oxazolones and the appropriate amino acid derivatives or heating it in the microwave for 5 min produced the target derivatives **8a, 8b, 9a, 10a and 10b** in a good yield. 1HNMR and 13CNMR identified the newly synthesized compounds, while the purity of the newly prepared compounds was checked by elemental analysis.

2.3. Biological Study

2.3.1. The study depended on causing ischemia followed by reperfusion (I/R) in the liver and ovary in rats and studying the protective effect of the test compound in comparison with NAC. I/R results in a series of pathophysiological events, including elevation in mitochondrial permeability, the release of cytochrome c, caspase-3 activation[32], the release of inflammatory mediators such as TNFα, IL-β,..etc., and the increase of oxidative stress that leads to apoptosis [33-35]. The decrease in tissue damage induced by I/R in a dose equivalent to 30 mg of NAC as an antiapoptotic reference [36-38]. The antiapoptotic mechanism was studied by biochemical, histological, immunohistochemical, and morphometric. Furthermore, serum biomarker concentrations were measured using suitable methods to detect liver and ovary injury. The biomarkers measured were either specific for each organ, liver and ovary or general for both as shown in **Table S1**. ***In vivo* antiapoptotic study in liver**

2.3.1.1. Assay of general biomarkers; (TNFα & MDA) inhibition and (SOD, GSH and NOx) activation in liver

2.3.1.2. Hepatic *in vivo* antiapoptotic study of compounds **8a, 8b, 9a, 10a** and **10b** based on the conc. And the percentage of inhibition for the liver general biomarkers TNFα and MDA compared to sham, model, and **NAC**. Complying with docking results, compounds **8a, and 10a** (with linker n=2 and *p*-methoxy or *p*-ethyl ester in ring A, respectively) displayed an excellent inhibitory effect on TNFα with 90.6 % and 90.47 %; respe,ctively in comparison with **NAC** (45.2 %) and on MDA with 90.77% and 88.1 % better than NAC (39%). Although compound **9a** (with linker n=2 and *p*- F in ring A) showed a moderate TNFα inhibitory effect (50.14%), it had better inhibition than NAC on MDA. Compounds 8b and 9a (with linker n = 5) also possessed a weak to no inhibition. Interestingly, compounds **8a, and 10a** showed excellent activation of SOD (98.57 % and 79.12%, respectively), GSH (101.33% and 98.5% respectively) and NOx (105.48 % and 96.46 %, respectively) greater than NAC (52.4%, 77% and 67.71%, respectively) as listed in **Table 1**. In contrast, compounds **9a**, **8b, and 10b** had a weak activation. These findings further support our hypothesis that compounds with short-chain linkers (n=2) are the best antiapoptotic compounds.

2.3.2.1 Assay of specific liver biomarkers (ALT and AST inhibition)

The liver-specific biomarkers (ALT and AST) were found in the case of apoptosis induction due to I/R. . Remarkably, compounds **8a** and **10a** demonstrated robust inhibition of ALT activity (93.62% and 99.17%, respectively) and AST activity (101.79% and 99.35%, respectively) when compared to NAC (42% and 27.5%, respectively) (**Table 2**).

2.3.2.2 Assay of specific ovarian biomarker (AMH)

Based on the results of general biomarkers estimations, it is predictable good antiapoptotic evidence on ovarian biomarkers. **8a, 10a** and **9a** revealed outstanding AMH activation (88.23% 110.6% and 109.41%, respectively) as listed in **Table 4**. Additionally, others with five carbon linker lengths were worth more than NAC. These experiments prove that some of the newly docked compounds will be good candidates as antiapoptotic agents. The above biochemical results for the ovary and liver match those observed before docking. Whereas **8a** and **10a** showed good binding with Cys285, which means more caspase-3 inhibition and less apoptosis, compounds with no interaction with Cys285 as in compounds 8a and 10b result in low caspase inhibition and more apoptosis. Moreover, **9a** showed excellent amelioration in the case of the ovary, which may be attributed to the fluorine group that probably enhances the lipophilicity of the drug, increasing the drug cell penetration.

Table 4: AMH concentrations in the ovary of I/R rats treated with 0 or 1.83 mM of **8a**, **8b**, **9a**, **10a**, **10b** and **NAC**.

Group	Serum AMH (ng/mol)	Activation %
Sham	2.18	100
Model	0.48	0
NAC	1.211	43
8a	1.98	**88.23**
8b	0.62	8.24
9a	2.34	**109.41**
10a	2.36	**110.6**
10b	0.70	12.94

***2.3.3* *In vivo* Antiapoptotic study in the ovary:**

2.3.3.1 Assay of general biomarkers; (SOD, GSH and NOx) activation and (MDA) inhibition in the ovary

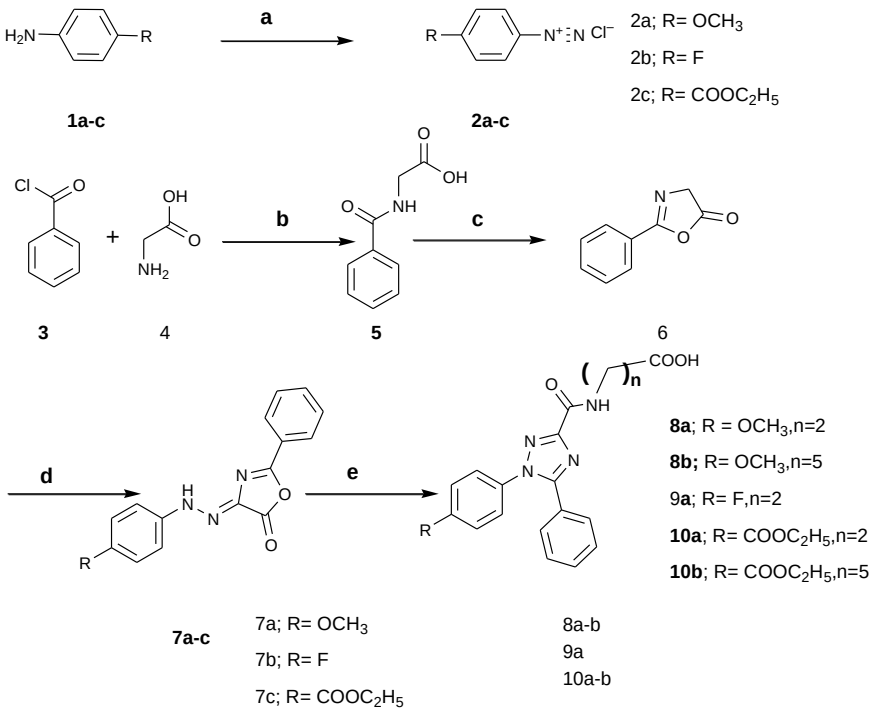

Reagents and conditions: (a) $NaNO_2$, HCl, stirring; (b) NaOH, HCl, stirring; (c) Ac_2O/ 60 °C; (d) compound (5a-e) NaOAc, 2-8 °C, 4h, stirring; (e) $H_2N(CH_2)nCOOH$ (n= 1,2,3,4), AcOH, NaOAc, reflux three h (55-60% yield) or microwave 3 min (80-85% yield)

Scheme 1: Synthesis of the target compounds **8a-b, 9a, 10a-b**

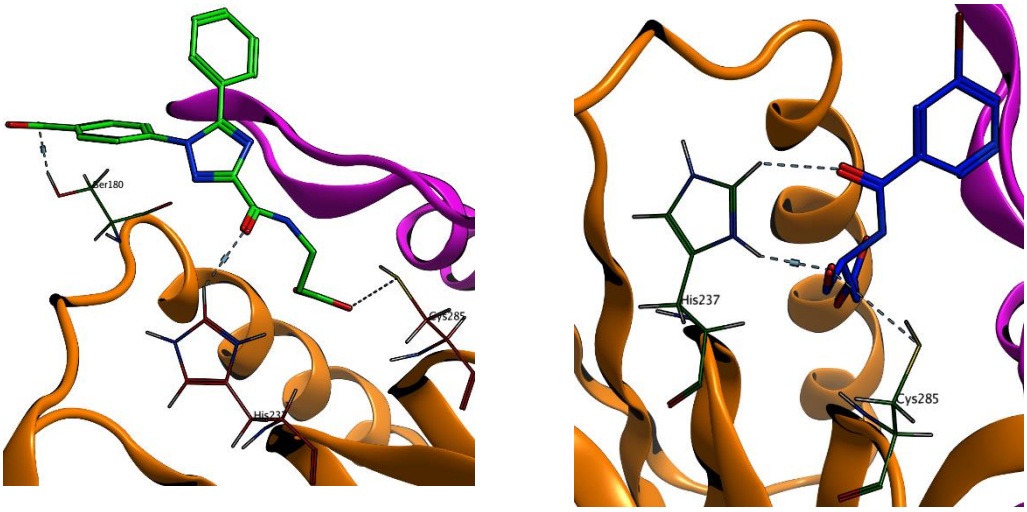

Figure 1: A 3D representation of the docking poses of compound **10a**(a) (green) and the co-crystallized ligand **NA3** (blue) in the caspase-3 catalytic site

Table 1: TNFα, MDA inhibition %, and SOD, GSH, and NOx activation in the liver of I/R rats treated with 0 or 1.83 mM of **8a**, **8b**, **9a**, **10a**, **10b** and **NAC**.

Biomarker		Sham[a]	Model[b]	NAC	8a	8b	9a	10a	10b
TNFα	Conc **(pg/mL)**	9.86	31.48	19.63	11.89	30.74	20.64	11.92	32.14

	% inhibition	100	0	45.2	**90.6**	3.4	50.14	**90.47**	-3.05
MDA	Conc (**nmol/g tissue**)	27.08	61.43	40.47	30.25	64.25	65.32	31.17	66.78
	% inhibition	100	0	39	**90.77**	-8.2	-11.32	**88.1**	-15.57
SOD	Conc **(nmol/mg protein)**	40.01	10.74	26.1	39.59	13.29	11.15	33.90	11.87
	% Activation	100	0	**52.4**	**98.57**	8.71	1.40	**79.12**	3.86
GSH	Conc **(µmol / mg protein)**	83.24	56.11	77.19	83.60	50.11	53.82	82.83	50.79
	% Activation	100	0	**77**	**101.33**	-22.12	-8.44	**98.5**	-19.61
NOx	Conc **(nmol/ gm tissue)**	141.79	83.6	123	145.19	80.57	81.68	139.73	79.60
	% Activation	100	0	67.71	**105.48**	-5.21	-3.3	**96.46**	-6.87

Sham[a] = No drug, without I/R Model[b] = No drug, with I/R

Table 2: The inhibition percent of ALT and AST in the liver of I/R rats treated with 0 or 1.83 mM of **8a**, **8b**, **9a**, **10a**, **10b** and **NAC**.

Group		**Sham[a]**	**Model[b]**	**NAC**	**11b**	**11d**	**13b**	**14b**	**14d**
ALT	Conc. (**U/I**)	28.55	69.6	45.75	31.17	72.26	70.64	29.89	70.46
	% inhibition	100	0	42	**93.62**	-6.48	-2.1	**99.17**	-13.86
AST	Conc. (**U/I**)	37.75	80.65	49.33	36.98	75.99	81.1	37.47	76.45
	% inhibition	100	0	27.5	**101.79**	10.87	9.8	**99.35**	-1.05

Sham[a] = No drug, without I/R Model[b] = No drug, with I/R

Table 3: SOD, GSH, and NOx concentrations in the ovary of I/R rats treated with 0 or 1.83 mM of **8b**, **8d**, **10b**, **11b**, **11d** and **NAC**.

Group	**Test**	**Sham[a]**	**Model[b]**	**NAC**	**8a**	**8b**	**9a**	**10a**	**10b**
SOD	Conc **(nmol/mg protein)**	142.01	65.93	109.45	133.11	73.22	136.29	140.97	69.22
	% Activation	100	0	**57.21**	**88.30**	9.6	**92.5**	**98.63**	4.32
GSH	Conc **(µmol / mg protein)**	44.95	25.51	41.84	46.35	22.28	45.87	47.03	23.77
	% Activation	100	0	**84**	**107.20**	-16.62	**104.37**	**110.7**	-8.95
NOx	Conc **(nmol/ gm tissue)**	171.61	105.92	145.33	168.42	107.45	170.24	165.34	100.51
	% Activation	100	0	**60**	**95.14**	2.33	**97.91**	**90.45**	-8.24
MDA	Conc (**nmol/g tissue**)	39.24	72.71	59.60	38.05	73.06	41.53	37.42	69.65
	Inhibition %	100	0	28	**103.56**	-1.05	**93.16**	**94.56**	9.14

Sham[a] = No drug, without I/R Model[b] = No drug, with I/R

The ovary was previously subjected to I/R to induce apoptosis. **Table 3** listed the results of **8a**, **10a** and **9a** (with linker n= 2) to exhibit again relatively significant activation for SOD (88.30 % 98.63% and 92.5 %, respectively), GSH (107.20% and 110.7%, 104.37 %, respectively) and NOx (95.14%, 90.45%, 97.91%, respectively). Moreover, they exhibited MDA inhibitory effects (103.56%, 94.56%and 93.16 %, respectively). On the other hand, **8b** and **10b** (with linker n= 5) possessed very weak activity. These findings provide further evidence for the suggested aspect; derivatives of short linkers showed the greatest antiapoptotic effect.

2.3.3.2. Assay of specific ovarian biomarker (AMH)

Based on the results of general biomarkers estimations, it is predictable good antiapoptotic evidence on ovarian biomarkers. **8a, 10a** and **9a** revealed outstanding AMH activation (88.23% 110.6% and 109.41%, respectively) as listed in **Table 4**. Additionally, others with five carbon linker lengths were worth more than NAC. These experiments prove that some of the newly docked compounds will be good candidates as antiapoptotic agents. The above biochemical results for the ovary and liver match those observed before docking. Whereas **8a** and **10a** showed good binding with Cys285, which means more caspase-3 inhibition and less apoptosis, compounds with no interaction with Cys285 as in compounds 8a and 10b result in low caspase inhibition and more apoptosis.

Moreover, **9a** showed excellent amelioration in the case of the ovary, which may be attributed to the fluorine group that probably enhances the lipophilicity of the drug, increasing the drug cell penetration.

Table 4: AMH concentrations in the ovary of I/R rats treated with 0 or 1.83 mM of **8a**, **8b**, **9a**, **10a**, **10b** and **NAC**.

Group	Serum AMH (ng/mol)	Activation %
Sham	2.18	100
Model	0.48	0
NAC	1.211	43
8a	1.98	**88.23**
8b	0.62	8.24
9a	2.34	**109.41**
10a	2.36	**110.6**
10b	0.70	12.94

2.4 Histopathological studies of liver and ovarian tissues

Hematoxylin and eosin (H& E) were used for histological examination while Perl's stain was used to detect iron [39, 40]. Activated caspase-3 immunohistochemistry was used as a marker for detecting apoptosis in tissue sections [41]. numerous apoptotic hepatocytic cells with intense reactions were detected by immunohistochemical study. This is in good harmony with previous researchers, who stated an increase in caspase-3 immunoreaction in the myocardium after six hours of ischemia [40]. The apoptotic histological changes observed in the present work were in accordance with previous studies that confirmed early damage of cells after reperfusion mainly in the form of apoptosis. They stated that numerous amounts of both cytochrome c and other apoptosis-enhancing molecules are released in ischemia-reperfusion, triggering the cells' apoptosis [42]. While Other researchers described apoptosis as a specific histological feature of cell death, characterized by shrunken cells, chromatin condensation, and nuclear fragmentation [43]. Some previous workers reported that increased lipid peroxidation that occurred during I/ R, led to the synthesis of both proteolytic lysosomal and mitochondrial matrix enzymes into the cytoplasm, leading to intracellular proteolysis and tissue damage [44]. Ovarian tissue that was taken from the sham group displayed a thin germinal layer covered the ovaries. It showed normal morphology with multiple follicles in various stages of development, ranging from primordial follicles to mature Graafian follicles. The growing follicles showed oocytes surrounded by distinct zona pellucida surrounding the oocytes. The Parenchymal ovarian cells surrounding the growing follicle are organized into concentric sheaths named theca folliculi. The secondary follicles were formed when little fluid-filled spaces between the granulosa cells appeared. when these spaces were enlarged and fused, they formed prominent mature Graafian follicles. The oocyte appeared peripherally in the follicle enclosed in the cumulus oophorus and surrounded by granulosa cells. Corpora lutea was also observed in lightly stained lutein cells between minimal connective tissue stroma (**Figure S8**).

In the current study, in the I/R group (model), the ovaries showed secondary follicles with intra-antral desquamated follicular cells, multiple atretic follicles without oocytes, and multiple dark nuclei. The corpora lutea appeared with hemorrhage and massive hemorrhage (**Figure S9**). These findings were under previous histological studies done on ischemic ovaries. These results are referred to the action of reactive oxygen species (ROS) formed during I/R. The I/R group exhibited massive interstitial hemorrhage and congested vessels in this work. It was in line with those who stated that torsion of the ovarian blood supply led to severe vascular congestion, hemorrhage, and eventually multiple necroses of ovarian tissue [45].

Using Perl's iron staining, it was found that intracellular cytoplasmic ferritin increased in the I/ R group, and it was in line found the same finding in the case of compounds **8a** and **10a**; this ferritin staining appeared more extensive if compared with the sham group and compounds **9a, 8b** and **10b**. Also, it was seen more than the I/ R group. It could be explained that ferritin H could suppress apoptotic cell death, with subsequently increasing tubular epithelial viability and improving function by limiting oxidative stress after I/R injury. In the present study, an immunohistochemical study for caspase-3 showed more markedly evident positive brownish staining for apoptosis, especially in follicular cells and interstitial cells in the I/R group if compared with the other groups. Previous researchers demonstrated that caspase-3 immunoreactivity was observed in the ovarian tissues in the I/R group and other groups. It was explained that apoptosis was performed by activating proteases called caspases, resulting in DNA fragmentation. The apoptotic process was detected by immune detecting active caspase-3. Furthermore, Caspase-3 enhances endogenous endonucleases that lead to DNA fragmentation.

2.4.1 H and E results for liver tissue (better to be before immune effect)

Sham sections of liver tissue stained with H&E revealed normal lobular architecture. The hepatocytes radiated as cords from the central veins. They had acidophilic cytoplasm and vesicular nuclei. Some hepatocytes appeared with two nucleoli. The blood sinusoids lay between the hepatic cells. The ischemic reperfusion (I/R) group showed that the hepatocytes had a variable amount of severe cytoplasmic vacuolations. Apoptotic cells were noticed in H&E staining (**Figure 2**).

2.4.1 Ovary

It is worth mentioning that both compounds **8a** and **10a** caused amelioration of all previous ovarian injuries caused by ischemic reperfusion injury if given before ischemia. The more or less standard lobular architecture was noticed. At the same time, the still variable amount of atretic follicles with the absence of its ova was seen. Furthermore, the corpora lutea appeared with minor hemorrhage (**Figure 3**).

H& E ovarian sections(**Figure S4 and S5**): Compound **9a** group showed a thick epithelial germinal layer covering ovarian tissue. Disturbed lobular architecture with congested blood vessels was also noticed. The focal ovarian stromal loss was seen. Stromal cells are arranged in clusters and show pale cytoplasm. Some ovarian follicles in this group displayed severe follicular cell loss without their ova. Multiple atretic follicles with separation of their follicular cells were detected. The corpora lutea showed degenerative features and appeared with congested blood vessels. H& E ovarian sections for compound **10b** showed disturbed ovarian lobular architecture. Stroma showed severe atretic follicles, dilated congested blood vessels, and interstitial hemorrhage. The proliferation of stromal cells was also noticed. Homogenous acidophilic material appeared in the ovarian stroma. Corpora lutea with severe vacuolations were frequently seen. Sever demarcations were seen between aggregated Corpora lutea **(Figure S6).**

2.4.2 Perl's staining results for liver and ovarian tissues.

By using Perl's iron staining (**Figure 4**), it was observed that intracellular cytoplasmic ferritin granules increased in the I/ R group, and it was per another researcher noticed the same finding. Using Perl's staining for compounds **8a** and **10a** groups, this ferritin staining was more intense and diffuse if compared with sham and I/R groups. It could be explained by Hatcher et al., who reported that ferritin H could decrease apoptotic cell death, with subsequent enhanced tubular epithelial viability and ameliorate renal function by limiting oxidative stress after I/R injury.

In the ovary, the sham group showed faint blue cytoplasmic staining, while the I/R group exhibited more blue cytoplasmic coloration compared with the sham group. Both compounds **8a** and **10a** group showed more cytoplasmic staining than a sham and previous I/R group. Compounds **8b,9a** and **10b** groups showed cytoplasmic staining less than **8a** and **10a** groups but still more than the sham group (**Figure S7**).

2.4.3 Immunohistochemical study for caspase-3 in the liver and ovary tissues.

An immunohistochemical study for caspase in the Sham group showed negative expression, while in the ischemic group, intense and massive hepatic cytoplasmic immunoreaction in liver cells was noticed. (**Figure S8**) In the ovary, an immunohistochemical study for caspase in the Sham group showed negative expression, while in the ischemic group, intense and massive ovarian cytoplasmic immunoreaction in ovarian cells was noticed. Regarding **9a, 8b**, and **10b** groups; the ovarian tissue showed more intense cytoplasmic and nuclear reactions than observed in the sham group. It was noticed that the **10a** and **8a** groups showed little cytoplasmic expression for caspase if compared with ischemic reperfusion, **9a, 8b**, and **10b (Figure S9).**

2.4.4 Morphometric studies for liver and ovary tissues.

For the morphometrical study; ten non-overlapping fields from three sections of each rat of all groups were used [46]. It was found that there was a high significance increase in liver cells immunostained for caspase-3 in the model group if compared with the sham group (P1<0.001). Additionally, it was a significant increase in liver cells immunoreactivity in **9a, 8b** and **10b** (p <0.001, P<0.001, P5<0.00) consequently if compared with the sham group. At the same time, there was a significant decrease in this expression in the case of **8a** and **10a** if compared with **9a, 8b** and **10b,** as shown in **Table S1.**

For ovary tissues, it was found that there was a high significance increase in ovarian cells immuno-stained for caspase-3 in the model group if compared with the sham group (P1<0.001). Additionally, it was a significant increase in ovarian cells immunoreactivity in both **9a, 8b** and **10b** (p <0.001, P<0.001, P5<0.00) consequently if compared with the sham group. At the same time, there was a significant decrease in this expression in the case of **8a** and **10a** if compared with **9a, 8b** and **10b,** as shown in **Table S1.**

2.5 Caspase-3 enzyme inhibition and selectivity assay

Caspase-3 enzyme inhibition IC_{50} assay was done in Vacsera using the ELISA method for the most active compounds **8a** and **10a**, which had 85137.62 ng/mL and 2432.82 ng/mL. So, the selectivity assay was done for **10a** toward other apoptotic caspases such as caspase 7, 8, 9, 10, and the IC_{50} equaled 6150.643 ng/mL, 884.7528 ng/mL, 35737 ng/mL, 1161.181 ng/mL.

3. Conclusion

A novel class of 1,5-diaryl triazole-3-carboxamide hybrid scaffolds was designed, synthesized, and characterized by

different spectroscopic techniques. The prepared compounds retain good-to-moderate caspase-3 inhibitory activity and possess substantial antiapoptotic activity. Our investigation unveiled that, among the synthesized target compounds, **8a and 10a** both possessing the shortest chain linker (n=2)- emerged as the most potent antiapoptotic candidates when compared to NAC. Furthermore, these compounds offered valuable insights into their robust caspase-3 inhibitory activity.. A detailed mechanistic study of molecular docking and biochemical and histopathological studies in the liver and the ovary prove this unexpectedly potent antiapoptotic activity that is expected to be a priority of future work.

4. Experimental

4.1 Chemistry

Chemicals were purchased from Aldrich, Alfa Aesar, Across Organics and El-Nasr Pharmaceutical Chemical Companies and used without further purification. The reaction progress was monitored using precoated TLC plates (Kiesslgel 60, 254 Merck); the spots were detected by exposure to a UV lamp at 254 nm. Analytical grade chemicals and solvents were used, and the progress of the reactions was monitored by thin-layer chromatography pre-coated Merck silica gel 60 F254 aluminum sheets. Melting points were determined on Stuart's electro-thermal melting point apparatus in degrees Celsius (^{C}) and were uncorrected. NMR spectra were recorded using Bruker AG (500 MHz ^{1}HNMR, 125 MHz ^{13}CNMR), Switzerland, Faculty of Pharmaceutical Sciences, Umm Al-Qura University, Mecca, Saudi Arabia and on Bruker Advance III (400 MHz ^{1}HNMR, 100 MHz ^{13}CNMR), Columbia, Vancouver, Canada; using TMS as an internal reference. Chemical shifts (δ) were expressed in ppm relative to TMS (δ=0 ppm) as the internal standard and $CDCl_3$ or DMSO-d_6 as a solvent. Chemical shifts (δ) were expressed in parts per million (ppm), and coupling constants (*J*) were expressed in Hertz. The signals were designated as follows: s, singlet; d, doublet; t, triplet; m, multiplet. Elemental analyses were recorded on Shimadzu GC/ MS-QP5050A, The Regional Center for Mycology and Biotechnology, Al-Azhar University, Egypt. The microwave device (household oven) was operated at maximum power.

4.1.1 General procedure for the synthesis of hippuric acid (5)

Benzoyl chloride (3.96 g, 0.028 mol) was added in three portions to a cold stirred solution of glycine (2.25g, 0.028 mol) in an aqueous sodium hydroxide (6 M, 15 mL). After each addition of benzoyl chloride, sodium hydroxide (6 M) was added to keep the pH between 7.4 and 8.0. The stirring was continued for about 2 h until a clear yellowish solution formed and then diluted hydrochloric acid was added in a portion-wise manner. The formed precipitate was filtered off, washed with water, air dried, and recrystallized in distilled water to afford white crystals of compound **5** (m.p: 187 – 189 ^{o}C) (reported: 187-188 ^{o}C) in 90% yield

General procedure for the syntheses of (*Z*)-2-Phenyl-4-(2-arylhydrazono)oxazol-5(4*H*)-one derivatives (7a,b,c) [48, 49]

Hippuric acid (0.013 mol, 3.50 g) in acetic anhydride (7 mL) was heated until a clear yellow solution was obtained; this solution was cooled to room temperature (solution A). To a cold solution of the *p*-substituted aniline derivatives (0.013 mol) in 5 N HCl (3 mL) in an ice-salt bath at 0-5°C, a solution of sodium nitrite (0.013 mol, 0.897 g) in the least amount of water was added in a dropwise manner. The reaction mixture was left for 10 min. (solution B). Solution A was added to solution B in the presence of anhydrous sodium acetate (0.018 mol, 1.5 g). The reaction mixture was stirred at 0-10°C for 2 h; the formed precipitate was filtered off, air-dried, and recrystallized from ethyl acetate affording the appropriate oxazolone derivatives in a good yield.

4-(2-(4-Methoxyphenyl)hydrazono)-2-phenyloxazol-5(4*H*)-one (7a)

Orange-red powder (yield: 85%, m.p: 205-206^{0}C, reported m.p: 201-203^{0}C)[50]

4-(2-(4-Fluorophenyl)hydrazono)-2-phenyloxazol-5(4H)-one (7b)

Deep orange powder (yield: 87%, m.p: 220-222^{o}C); ^{1}H NMR (500 MHz, DMSO-d_6) δ(ppm): 11.84 (s, 1H, NH), 8.12-8.09 (m, 2H, ArH), 7.73-7.70 (m, 1H, ArH), 7.65-7.60 (m, 2H, ArH), 7.50-7.45 (d, 2H, ArH), 7.24-7.21 (m, 2H, ArH); ^{13}C NMR (125MHz, DMSO-d_6) δ(ppm): 161.72, 159.87, 157.96, 139.83, 134.06, 132.16, 129.83, 128.28, 125.83, 117.09, 116.53; DEPT^{13}C NMR (125MHz, DMSO-d_6) δ(ppm): 134.06, 129.83, 128.28, 117.09, 116.53.

Ethyl-4-(2-(5-oxo-2-phenyloxazol-4(5H)-ylidene) hydrazinyl) benzoate (7c)

Orange powder (yield 86%, m.p: 209-210 ^{o}C);^{1}H NMR (500 MHz, DMSO-d_6) δ(pm): 12.66 (bs, 1H, OH), 11.98 (s, 1H, NH), 8.86 (s, 1H, NH), 8.02 – 7.87 (m, 3H, ArH), 7.83 – 7.72 (m, 2H, ArH), 7.59 – 7.47 (m, 4H, ArH), 4.39-4.34 (m, 2H, CH_2), 1.35-1.29 (m, 3H, CH_3); ^{13}C NMR (125 MHz, DMSO-d_6) δ(ppm): 166.93, 163.15, 147.19, 134.28, 131.91, 131.33, 129.90, 129.05, 128.84, 128.56, 127.70, 114.95, 60.87, 14.73; DEPT^{13}C NMR (125 MHz, DMSO-d_6) δ(ppm): 131.91, 131.33,128.56, 127.70, 114.95, 60.87, 14.73

General procedure of *p*-substituted (1,5-diaryl-1*H*-1,2,4 triazole-3-carboxamido) acid derivatives (8a,8b), 9a, (10a, 10b)[51, 52]

A mixture of oxazolone derivatives (0.01 mol), the appropriate amino acid analogs (0.012 mol), and

anhydrous sodium acetate (0.50g) are dissolved in acetic acid glacial (15 mL). The reaction mixture was heated under reflux for 3 h or under the microwave; the reaction ran for 5 minutes (divided into 30 sec for each run to prevent explosive of solvent) and was left to cool in the air. The reaction mixture was then diluted with ice water (4 mL for each 1 mL acetic acid). The precipitate was filtered off, washed with water, and re-crystallized from toluene to obtain white crystals.

3-(1-(4-Methoxyphenyl)-5-phenyl-1*H*-1,2,4-triazole-3-carboxamido)propanoic acid (8a)

White crystals; (r = 53% yield, MW = 76%) ; mp: 160°C; ^{1}H NMR (500 MHz, $CDCl_3$) δ (ppm): 8.09 (bs, 1H, NH), 7.50 (d, *J* = 7.5 Hz, 2H, ArH), 7.45 (t, J = 7.5 Hz, 1H, ArH), 7.40 – 7.35 (m, 2H, ArH), 7.31–7.27 (m, 2H, ArH), 6.93 (d, *J* = 7.5 Hz, 2H, ArH), 3.86 (s, 3H, OCH_3), 3.82–3.78 (m, 2H, CH_2NH), 2.76–2.73 (m, 2H, CH_2C=O); ^{13}C NMR (125 MHz, $CDCl_3$) δ (ppm): 176.13, 160.24, 159.19, 155.71, 154.84, 130.69, 130.33, 129.06, 128.73, 126.90, 126.47, 114.57, 55.60, 34.98, 33.78; Anal. Calcd for $C_{19}H_{18}N_4O_4$ (366.38): C, 62.29; H, 4.95; N, 15.29; Found; C, 62.05; H, 5.13; N, 15.47.

6-(1-(4-Methoxyphenyl)-5-phenyl-1*H*-1,2,4-triazole-3-carboxamido)hexanoic acid (8b)

White crystals; (r = 72% yield, MW = 87%, mp: 95°C); ^{1}H NMR (400 MHz, $CDCl_3$) δ (ppm): 9.41 (s, 1H, OH), 7.51 (d, *J* = 7.5 Hz, 2H, ArH), 7.47 (t, *j* = 6.8 Hz, 1H, NH), 7.43 – 7.37 (m, 2H, ArH), 7.36 – 7.28 (m, 3H, ArH), 6.92 (d, *J* = 7.5 Hz, 2H, ArH), 3.84 (s, 3H, OCH_3), 3.50 (q, *j* = 6.8 Hz, 2H, CH_2NH), 2.36 (t, *J* = 7.2 Hz, 2H, CH_2C=O), 1.74 – 1.52 (m, 4H, $2CH_2$), 1.56 – 1.19 (m, 2H, CH_2CH_2); ^{13}C NMR (100 MHz, $CDCl_3$) δ (ppm): 178.63, 160.21, 159.05, 155.99, 154.67, 130.58, 130.47, 128.98, 128.69, 126.90, 126.70, 114.56, 55.60, 39.28, 33.87, 29.19, 26.32, 24.36; Anal. Calcd for $C_{22}H_{24}N_4O_4$ (408.46): C, 64.69; H, 5.92; N, 13.72; Found; C, 64.97; H,6.09; N,14.01.

3-(1-(4-Fluorophenyl)-5-phenyl-1*H*-1,2,4-triazole-3-carboxamido)propanoic acid (9a)

White crystals; (r = 62% yield, MW = 88%, m.p = 153°C); ^{1}H NMR (400 MHz, DMSO-d_6) δ (ppm) : 12.33 (bs, 1H, COOH), 8.68 (t, *J* = 5.6 Hz, 1H, $NHCH_2$), 7.59–7.54 (m, 2H, ArH), 7.51–7.47 (m, 3H, ArH), 7.47–7.43 (m, 2H, ArH), 7.4–7.37 (m, 2H, ArH), 3.50 (q, *J* = 6.8 Hz, 2H,CH_2 NH), 2.56–2.51 (m, 2H, CH_2C=O); ^{13}C NMR (125 MHz, DMSO-d_6) δ (ppm): 173.45, 163.59, 161.78, 158.98, 156.66, 155.17, 130.95, 129.30, 129.16, 128.99, 127.34, 117.11, 35.48, 34.22; Anal.Calcd for $C_{18}H_{15}FN_4O_3$ (354.34): C, 61.01; H, 4.27; N, 15.81; Found C, 61.26; H, 4.45; N, 16.07.

3-(1-(4-(ethoxycarbonyl)phenyl)-5-phenyl-1*H*-1,2,4-triazole-3-carboxamido)propanoic acid (10a)

White crystals; (r = 74% yield, MW = 89%, m.p = 164°C); ^{1}H NMR (400 MHz, $CDCl_3$) δ (ppm): 8.09 (d, *J* = 6.8 Hz, 2H, ArH), 8.01 (t, *J* = 6.0 Hz, 1H, $NHCH_2$), 7.53–7.46 (m, 2H, ArH), 7.46–7.41 (m, 3H, ArH), 7.39 (d, *J* = 6.8 Hz, 2H, Ar. H), 4.41 (q, *J* = 7.2 Hz, 2H, OCH_2CH_3), 3.84–3.76 (m, 2H, CH_2CH_2NH), 2.74 (t, *J* = 6.0 Hz, 2H,CH_2C=O), 1.41 (t, *J* = 7.2 Hz, 3H, CH_3CH_2); ^{13}C NMR (100 MHz, $CDCl_3$) δ (ppm): 176.29, 165.34, 159.03, 156.40, 155.23, 140.74, 131.24, 131.00, 130.76, 129.11, 128.91, 126.37, 125.08, 61.56, 35.00, 33.75, 14.27; Anal. Calcd for $C_{21}H_{20}N_4O_5$ (408.41): C, 61.76; H, 4.94; N, 13.72; Found C, 61.54; H, 5.03; N, 14.01.

6-(1-(4-(Ethoxycarbonyl)phenyl)-5-phenyl-1*H*-1,2,4-triazole-3- carboxamido)hexanoic acid (10b)

White crystals; (r = 53% yield, MW = 67%, m.p = 145°C); ^{1}H NMR (500 MHz, DMSO-d_6) δ (ppm): 11.98 (s, 1H,COOH), 8.67 (bs, 1H, NH), 8.05 (d, *J* = 7.0 Hz, 2H, ArH), 7.59 (d, *J* = 7.0 Hz, 2H, ArH),7.50–7.48 (m, 3H, ArH), 7.46–7.44 (m, 2H, ArH), 3.32–3.25 (m, 4H, OCH_2 and CH_2NH), 2.24-2.20 (m, 2H, CH_2C=O), 1.56-1.50 (m, 6H, $3CH_2$), 1.34-1.28 (m, 3H,CH_2CH_3); ^{13}C NMR (125 MHz, DMSO-d_6) δ (ppm): 174.96, 166.85, 158.92, 157.28, 155.14, 141.17, 132.07, 131.07, 131.00, 129.42, 129.22, 127.38, 126.28, 61.54, 39.06, 34.08, 29.30, 26.42, 24.71, 14.56; Anal. Calcd for $C_{24}H_{26}N_4O_5$ (450.50): C, 63.99; H, 5.82; N, 12.44; Found C, 64.15; H, 5.97; N, 12.70.

4.2 Docking study

The 3D of caspase-3 was obtained from Protein Data Bank (https://www. rcsb. org/; PDB ID code: 1re1). Protein contains a reference molecule called nicotinic acid succinic semialdehyde derivative (NA3) as a co-crystallized ligand. The protein binding sites were managed using modules of Ligand Atoms Selection of MOE, and the **NA3** binding sites were used in the crystal structure as a reference. The sequence order of the binding sites was set using the MOE program. Hydrogen was added to complete the protein structure using selected Protonate 3D of the MOE program; only ligand and protein chains A and B of the crystal structure were used. The protein was then aligned using Align module of MOE. For the docking simulation process, the placement was managed on a triangular matcher, rescoring was managed on the London dG parameter, and the conformation number was managed in 5 poses with 30 refinements; conformation was selected as the forcefield of MOE and was used to generate five poses. All the docking conformations were analyzed, and the best value with the particular pose was selected for further interactional study.

4.3 Biology

Sera were separated and stored in aliquots at 80 °C till used for estimation of liver transaminases, including alanine transaminase (ALT) and aspartate transaminase (AST) by enzymatic colorimetric methods using commercial kits (spectrum diagnostic, Cairo, Egypt). MDA, an index of lipid peroxidation, was determined by using1,1,3 tetra methoxy propane as standard [53]. A

tumor necrosis factor (TNFα) ELISA kit (IDlabsT- Minc. Biotechnology, Canada) was used. Anti-Mullerian Hormone (AMH) ELISA kit (Abcam, USA) was utilized.

Total NOx, the stable oxidation end product of nitric oxide, served as an index of nitric oxide level and was measured by reduction of nitrate into nitrite using activated cadmium granules, followed by color development with Griess reagent in an acidic medium [54].

The activity of SOD was measured by the method with a slight modification. This method depends on the inhibition of the pyrogallol autooxidation by SOD. Calculating the percentage of inhibition for the samples was done by running a control with no sample under the same conditions. [55] SOD activity was expressed in units; where the unit equals the amount of the enzyme that inhibited 50% of pyrogallol autoxidation.

The percentage of activation or inhibition is calculated as follows:[56]

Calculation % of activation = [(**X**-min)/(max-min)] x 100

Calculation % of inhibition = 1-[(**X**-min)/(max-min)] x 100

X = specific conc. (U/I), **min** = least conc., **max** = last conc

4.4 Caspase inhibition assay method

Using abcam kits for caspases

4.5 Histology

4.5.1 Material and Methods

Ovarian specimens were obtained from each group and fixed in 10% formol saline for 24 h. Paraffin blocks were carried on, and 5-µm thick sections were subjected to H&E, Perls' stain. Other sections were further used for immunohistochemical study.

4.5.2 Immunohistochemical study

The caspase-3 antibody is a rabbit polyclonal for staining formalin-fixed paraffin-embedded tissues (Biovision, Milpitas, California, USA). The primary antibody (diluted at 1:20) was applied to the sections for 60 min. Then, the sections were incubated with the secondary antibody (biotinylated rabbit polyclonal antibody). The reaction was visualized with diaminobenzidine tetrahydrochloride and was noticed to be cytoplasmic. Sections were then counterstained with Mayer's hematoxylin.

4.5.3 Image capture

Histological sections were captured using Olympus digital camera mounted on a BX51 microscope (Olympus, Japan) connected to a computer programmed with LC micro application software in the light microscopic unit of the Histology Department, Faculty of Medicine, Minia University. Images were saved as jpg. Adobe Photoshop 7 standardizes brightness, contrast, and background color.

4.5.4 Morphometric analysis

Quantitative data were collected to measure the mean number of immune-stained cells for caspase. Measurements were performed in 8 randomly selected non-overlapping fields from the rat of each group under magnification X 400.

4.5.5 Data handling and Statistical analysis

Quantitative data were analyzed using SPSS (IBM Corp. Released 2010. Windows, Version 19.0). The mean and standard error (SE) was calculated for the parameters of each group. Values were expressed as means ±SE. One-way analysis of variance (ANOVA) test was carried out to estimate significant differences between groups, followed by Tukey-Kramer as a post hoc test. The results were considered statistically significant if the p-values were <0.05.

Conflicts of Interest

The authors declare no conflict of interest

Supplementary File

https://odr.journals.ekb.eg/article_357547.html

References

[1] Vo, T.T. and A. Letai, *BH3-only proteins and their effects on cancer.* Adv Exp Med Biol, 2010. **687**: p. 49-63.

[2] Norbury, C.J. and I.D. Hickson, *Cellular responses to DNA damage.* Annu Rev Pharmacol Toxicol, 2001. **41**: p. 367-401.

[3] Pu, X., et al., *Caspase-3 and caspase-8 expression in breast cancer: caspase-3 is associated with survival.* Apoptosis, 2017. **22**(3): p. 357-368.

[4] Wang, C.-C., et al., *Caspase-1 inhibitor ameliorates experimental autoimmune myasthenia gravis by innate dendric cell IL-1-IL-17 pathway.* Journal of neuroinflammation, 2015. **12**(1): p. 118.

[5] Akpan, N.E., *The intrinsic caspase death pathway in stroke neurodegeneration*. 2013: Columbia University.

[6] Wang, X.-J., et al., *Activation and regulation of caspase-6 and its role in neurodegenerative diseases.* Annual review of pharmacology and toxicology, 2015. **55**: p. 553-572.

[7] Singh, P.K. and A. Kumar, *Mitochondria mediates caspase-dependent and independent retinal cell death in Staphylococcus aureus endophthalmitis.* Cell death discovery, 2016. **2**(1): p. 1-11.

[8] Sun, C., et al., *MicroRNA-98 negatively regulates myocardial infarction-induced apoptosis by down-regulating Fas and caspase-3.* Scientific reports, 2017. **7**(1): p. 1-11.

[9] Woolbright, B.L., W.-X. Ding, and H. Jaeschke, *Caspase inhibitors for the treatment of liver disease: friend or foe?* 2017, Taylor & Francis.

[10] Aziz, M., A. Jacob, and P. Wang, *Revisiting caspases in sepsis.* Cell death & disease, 2014. **5**(11): p. e1526-e1526.

[11] Hwang, H.S. and H.A. Kim, *Chondrocyte apoptosis in the pathogenesis of osteoarthritis.* International journal of molecular sciences, 2015. **16**(11): p. 26035-26054.

[12] Malysheva, I., et al. *The level of cytokines and expression of caspase genes in rheumatoid arthritis*. in *Doklady Biochemistry and Biophysics*. 2016. Springer.

[13] Qi, X., et al., *Critical role of caspase-8-mediated IL-1 signaling in promoting Th2 responses during asthma pathogenesis.* Mucosal immunology, 2017. **10**(1): p. 128-138.

[14] Aly, A.A., et al., *New quinoline-2-one/pyrazole derivatives; design, synthesis, molecular docking, anti-apoptotic evaluation, and caspase-3 inhibition assay.* Bioorganic chemistry, 2020. **94**: p. 103348.

[15] Slee, E.A., C. Adrain, and S.J. Martin, *Executioner caspase-3,-6, and-7 perform distinct, non-redundant roles during the demolition phase of apoptosis.* Journal of biological Chemistry, 2001. **276**(10): p. 7320-7326.

[16] Walsh, J.G., et al., *Executioner caspase-3 and caspase-7 are functionally distinct proteases.* Proceedings of the National Academy of Sciences, 2008. **105**(35): p. 12815-12819.

[17] Guo, G., et al., *Clinical features of ischemic hepatitis caused by shock with four different types: a retrospective study of 328 cases.* International journal of clinical and experimental medicine, 2015. **8**(9): p. 16670.

[18] Legro, R.S., *Evaluation and Treatment of Polycystic Ovary Syndrome*, in *Endotext*, K.R. Feingold, et al., Editors. 2000, MDText.com, Inc.: South Dartmouth (MA).

[19] Teede, H., A. Deeks, and L. Moran, *Polycystic ovary syndrome: a complex condition with psychological, reproductive and metabolic manifestations that impacts on health across the lifespan.* BMC medicine, 2010. **8**(1): p. 41.

[20] Ndefo, U.A., A. Eaton, and M.R. Green, *Polycystic ovary syndrome: a review of treatment options with a focus on pharmacological approaches.* Pharmacy and Therapeutics, 2013. **38**(6): p. 336.

[21] Onder, A., et al., *The protective effects of curcumin on intestine and remote organs against mesenteric ischemia/reperfusion injury.* Turk J Gastroenterol, 2012. **23**(2): p. 141-7.

[22] Shi, Y., *Caspase activation, inhibition, and reactivation: a mechanistic view.* Protein science, 2004. **13**(8): p. 1979-1987.

[23] Ganesan, R., et al., *Exploring the S4 and S1 prime subsite specificities in caspase-3 with aza-peptide epoxide inhibitors.* Biochemistry, 2006. **45**(30): p. 9059-9067.

[24] Seaman, J., et al., *Cacidases: caspases can cleave after aspartate, glutamate and phosphoserine residues.* Cell Death & Differentiation, 2016. **23**(10): p. 1717-1726.

[25] Ng, S.L., et al., *"Click" synthesis of small-molecule inhibitors targeting caspases.* Organic & biomolecular chemistry, 2008. **6**(5): p. 844-847.

[26] Kumar, S.P. and P.C. Jha, *Multi-Pharmacophore Modeling of Caspase-3 Inhibitors using Crystal, Dock and Flexible Conformation Schemes.* Combinatorial chemistry & high throughput screening, 2018. **21**(1): p. 26-40.

[27] Sulpizi, M., U. Rothlisberger, and P. Carloni, *Molecular dynamics studies of caspase-3.* Biophysical journal, 2003. **84**(4): p. 2207-2215.

[28] Ramírez, D. and J. Caballero, *Is it reliable to take the molecular docking top scoring position as the best solution without considering available structural data?* Molecules, 2018. **23**(5): p. 1038.

[29] Fisk, J.S., R.A. Mosey, and J.J. Tepe, *The diverse chemistry of oxazol-5-(4 H)-ones.* Chemical Society Reviews, 2007. **36**(9): p. 1432-1440.

[30] Grzetic, J. and J. Oomens, *Spectroscopic evidence for an oxazolone structure in anionic b-type peptide fragments.* Journal of the American Society for Mass Spectrometry, 2011. **23**(2): p. 290-300.

[31] Wang, H., *Comprehensive Organic Name Reactions*. 2010: Wiley.

[32] Gong, L., et al., *RTN1-C mediates cerebral ischemia/reperfusion injury via ER stress and mitochondria-associated apoptosis pathways.* Cell death & disease, 2017. **8**(10): p. e3080-e3080.

[33] Datta, G., B.J. Fuller, and B.R. Davidson, *Molecular mechanisms of liver ischemia reperfusion injury: insights from transgenic knockout models.* World journal of gastroenterology: WJG, 2013. **19**(11): p. 1683.

[34] Collard, C.D. and S. Gelman, *Pathophysiology, clinical manifestations, and prevention of ischemia-reperfusion injury.* Anesthesiology: The Journal of the American Society of Anesthesiologists, 2001. **94**(6): p. 1133-1138.

[35] Kalogeris, T., et al., *Ischemia/reperfusion.* Comprehensive Physiology, 2011. **7**(1): p. 113-170.

[36] D'Amico, F., et al., *Use of N-acetylcysteine during liver procurement: a prospective randomized controlled study.* Liver Transpl, 2013. **19**(2): p. 135-44.

[37] Zhang, F., et al., *The anti-apoptotic effects of N-acetylcysteine in neonatal rat cardiomyocytes underwent hypoxia-reoxygenation injury.* Zhonghua xin xue guan bing za zhi, 2010. **38**(5): p. 445-449.

[38] Sun, Y., et al., *N-acetylcysteine attenuates reactive-oxygen-species-mediated endoplasmic reticulum stress during liver ischemia-reperfusion injury.* World Journal of Gastroenterology: WJG, 2014. **20**(41): p. 15289.

[39] Fischer, A.H., et al., *Hematoxylin and eosin staining of tissue and cell sections.* Cold spring harbor protocols, 2008. **2008**(5): p. pdb. prot4986.

[40] Han, S., et al., *Hepatic iron overload is associated with hepatocyte apoptosis during Clonorchis sinensis infection.* BMC infectious diseases, 2017. **17**(1): p. 531.

[41] Duan, W.R., et al., *Comparison of immunohistochemistry for activated caspase-3 and cleaved cytokeratin 18 with the TUNEL method for quantification of apoptosis in histological sections of PC-3 subcutaneous xenografts.* The Journal of Pathology: A Journal of the Pathological Society of Great Britain and Ireland, 2003. **199**(2): p. 221-228.

[42] Hirakawa, A., et al., *Mitochondrial permeability transition and cytochrome c release in ischemia-reperfusion injury of the rat liver.* Journal of Surgical Research, 2003. **111**(2): p. 240-247.

[43] Galluzzi, L., et al., *Molecular mechanisms of cell death: recommendations of the Nomenclature Committee on Cell Death 2018.* Cell Death & Differentiation, 2018. **25**(3): p. 486-541.

[44] Ayala, A., M.F. Muñoz, and S. Argüelles, *Lipid peroxidation: production, metabolism, and signaling mechanisms of malondialdehyde and 4-hydroxy-2-nonenal.* Oxidative medicine and cellular longevity, 2014. **2014**.

[45] Abdel-Gaber, S., et al., *Ameliorative effect of nicorandil in ovarian ischemia-reperfusion-induced injury in rats: role of potassium channel.* Naunyn-Schmiedeberg's archives of pharmacology, 2020.

[46] Hafez, S.M.N.A., *Age related changes in the dermal mast cells and the associated changes in the dermal collagen and cells: A histological and electron microscopy study.* Acta histochemica, 2019. **121**(5): p. 619-627.

[47] Ahluwalia, V. and S. Dhingra, *Comprehensive Practical Organic Chemistry: Qualitative Analysis*. 2004: Universities Press.

[48] Mustafa, M., et al., *Synthesis, antiproliferative, anti-tubulin activity, and docking study of new 1, 2, 4-triazoles as potential combretastatin analogues.* European journal of medicinal chemistry, 2017. **141**: p. 293-305.

[49] Nilsson, E.E., et al., *Inhibitory actions of Anti-Müllerian Hormone (AMH) on ovarian primordial follicle assembly.* PloS one, 2011. **6**(5).

[50] Hagedoorn, J., B. Lokshin, and S. Malo, *Alliances and the innovation performance of corporate and public research spin-off firms.* Small Business Economics, 2018. **50**(4): p. 763-781.

[51] Shida, T., et al., *1, 5-diphenyl-1H-1, 2, 4-triazole-3-carboxamide derivatives and herbicidal composition containing the same*. 1990, Google Patents.

[52] Aboeldahab, A.M., et al., *Spirohydantoins and 1, 2, 4-triazole-3-carboxamide derivatives as inhibitors of histone deacetylase: Design, synthesis, and biological evaluation.* European journal of medicinal chemistry, 2018. **146**: p. 79-92.

[53] Buege, J.A. and S.D. Aust, *[30] Microsomal lipid peroxidation*, in *Methods in enzymology*. 1978, Elsevier. p. 302-310.

[54] Söğüt, S., et al., *Changes in nitric oxide levels and antioxidant enzyme activities may have a role in the pathophysiological mechanisms involved in autism.* Clinica Chimica Acta, 2003. **331**(1-2): p. 111-117.

[55] Luoma, J.S., et al., *Expression of extracellular SOD and iNOS in macrophages and smooth muscle cells in human and rabbit atherosclerotic lesions: colocalization with epitopes characteristic of oxidized LDL and peroxynitrite-modified proteins.* Arteriosclerosis, thrombosis, and vascular biology, 1998. **18**(2): p. 157-167.

[56] Li, A.P., *ADME-tox screening in drug discovery*, in *Integrated drug discovery technologies*. 2002, Marcel Dekker New York. p. 289-318.